Effect of molecular alignment and orientation on elliptically polarized high-order harmonic generation

Ru Zhang,[1] Feng Wang,[1,*] Hua Yuan,[2,†] Shiju Chen,[2] Chunhui Yang,[1] Tianxin Ou,[1] Jiahang Song,[2] Qing Liao,[1,‡] and Peixiang Lu[3]

[1]*Hubei Key Laboratory of Optical Information and Pattern Recognition, Wuhan Institute of Technology, Wuhan 430205, China*

[2]*School of Physics and Optoelectronic Engineering, Shandong University of Technology, Zibo 255049, China*

[3]*Guangdong Intelligent Robotics Institute, Dongguan 523808, China*

(Received 17 August 2023; revised 31 January 2024; accepted 11 April 2024; published 26 April 2024)

We present a theoretical investigation of the influence of molecular alignment and orientation on elliptically polarized high-order harmonic generation (HHG) from CO molecules exposed to a linearly polarized pulse. The results show that the ellipticity of HHG observed in a partially aligned or oriented CO molecular ensemble significantly deviates from that of the individual response. Additionally, we find that the ellipticity of HHG in the CO molecular ensemble exhibits strong dependence on the degree of molecular alignment/orientation as well as the time delay between the alignment/orientation and probe pulses. More importantly, under the proper alignment/orientation angle, a large HHG ellipticity can be achieved from the partially aligned/oriented molecular ensemble at a moderate degree of alignment/orientation. These findings relax the experimental requirement of a high degree of molecular alignment/orientation for harmonic generation with large ellipticity.

DOI: 10.1103/PhysRevA.109.043118

I. INTRODUCTION

High-order harmonic generation (HHG) is a highly nonlinear, nonperturbative process occurring in atoms or molecular media subject to intense laser fields [1,2]. Due to its excellent coherence and extremely wide plateau structure, HHG has provided an effective way to generate the coherent attosecond pulses [3,4]. These attosecond pulses have enabled the detection and manipulation of electronic dynamic processes in atoms, molecules, and condensed matter with unparalleled temporal and spatial resolution [5–9]. Additionally, HHG also serves as an ideal source for generating the extreme ultraviolet [10] and soft x-ray radiations [11].

Recently, elliptically polarized (EP) harmonics have emerged as a subject of extensive interest, driven by their applications in studying ultrafast chiral-specific dynamics in molecules [12], x-ray magnetic circular dichroism spectroscopy [13], and structural properties of materials [14]. To generate EP harmonics, various methods have been proposed, falling into two categories. The first is to employ different driving laser fields, such as the EP pulse [15–17], the orthogonal two-color field [18,19], the two-color cross-linearly polarized laser field [20,21], the two-color counter-rotating circularly polarized (CP) laser field [22,23], the noncollinear CP laser field [24–26], polarization gating [27], and so on. The second is to choose special target media, such as the ring-current states [28,29], mixed gases [30], and molecules [31]. Among the methods, the interaction of linearly polarized pulse with molecules is a traditional approach. Molecules have a rich internal structure, which has been demonstrated to significantly affect the ellipticity of HHG. For example, Son *et al.* [32] found that the two-center interference can induce the EP HHG from H_2^+. Du *et al.* [33] demonstrated that the asymmetry of the highest occupied molecular orbital (HOMO) of a CO molecule can give rise to a large ellipticity of HHG. Smirnova *et al.* [34] found that the channel interference of a CO_2 molecule can result in an increased ellipticity of HHG. In addition, for an individual molecule, the ellipticity of HHG has also been demonstrated to depend sensitively on the alignment/orientation angle between the molecular axis and laser polarization [33,35]. To realize the molecular alignment/orientation in experiments, researchers have developed several techniques. The usage of an intense femtosecond laser pulse is an extensively used approach for realizing the molecular alignment [36–39]. By precisely adjusting the intensity and duration of the laser pulse, the degree of molecular alignment can be effectively improved [40]. Compared with molecular alignment, controlling molecular orientation is more challenging. Some methods including the two-color laser field [41,42], a terahertz few-cycle laser field [43,44], a half-cycle laser field [45,46], and an intense laser field combined with a weak dc electric field [47–49] have been employed to realize the molecular orientation. However, despite these efforts, achieving a perfect molecular alignment/orientation in experiments remains an ongoing challenge [50–52]. For the partially aligned/oriented molecular ensemble, the measurement is a result averaged over the molecular alignment/orientation distribution. In the past, Zhou *et al.* [31] experimentally and Le *et al.* [53] theoretically studied the harmonic ellipticity of N_2 molecules with different molecular alignment angles at a specific alignment degree. However, it is essential to elucidate the influence of imperfect molecular alignment/orientation on EP HHG.

*wangfeng@wit.edu.cn
†yuanhua@sdut.edu.cn
‡liaoqing@wit.edu.cn

In this work, we calculate the EP HHG resulting from the interaction between the CO molecular ensemble and a linearly polarized pulse to explore the influence of molecular alignment and orientation on EP HHG. We find that the molecular alignment and orientation significantly affect the ellipticity of HHG. By adjusting the alignment or orientation angle, we demonstrate that the EP HHG with large ellipticity (approximately 0.98) can be obtained from a partially aligned/oriented molecular ensemble under the appropriate experimental condition for molecular alignment/orientation.

II. THEORETICAL MODEL

A. Lewenstein model

The HHG radiation for an individual CO molecule was calculated by the Lewenstein model [54]. The parallel and perpendicular components of time-dependent dipole momentum are described as

$$\begin{aligned} D_{\parallel}(t,\beta) = i\int_{-\infty}^{t} dt' \left[\frac{\pi}{\xi + i(t-t')/2}\right]^{3/2} \\ \times \{\cos(\beta) d_x[\mathbf{p}_{\rm st}(t',t) - \mathbf{A}(t')] \\ + \sin(\beta) d_y[\mathbf{p}_{\rm st}(t',t) - \mathbf{A}(t')]\} \\ \times \{\cos(\beta) d_x^*[\mathbf{p}_{\rm st}(t',t) - \mathbf{A}(t)] \\ + \sin(\beta) d_y^*[\mathbf{p}_{\rm st}(t',t) - \mathbf{A}(t)]\} \\ \times e^{-iS_{\rm st}(t',t)} E(t') g(t') + \text{c.c.}, \end{aligned} \tag{1}$$

$$\begin{aligned} D_{\perp}(t,\beta) = i\int_{-\infty}^{t} dt' \left[\frac{\pi}{\xi + i(t-t')/2}\right]^{3/2} \\ \times \{\sin(\beta) d_x[\mathbf{p}_{\rm st}(t',t) - \mathbf{A}(t')] \\ - \cos(\beta) d_y[\mathbf{p}_{\rm st}(t',t) - \mathbf{A}(t')]\} \\ \times \{\sin(\beta) d_x^*[\mathbf{p}_{\rm st}(t',t) - \mathbf{A}(t)] \\ - \cos(\beta) d_y^*[\mathbf{p}_{\rm st}(t',t) - \mathbf{A}(t)]\} \\ \times e^{-iS_{\rm st}(t',t)} E(t') g(t') + \text{c.c.} \end{aligned} \tag{2}$$

Here, $\mathbf{A}(t')$ is the vector potential of the probe pulse $E(t')$, linearly polarized on the x-y plane with an angle β with respect to the molecular axis as shown in Fig. 1(d). ξ is a positive regularization constant. $g(t',\beta) = \exp[-\int_{-\infty}^{t} w(t',\beta)dt']$ is the ground-state amplitude at the time t with $w(t',\beta)$ of the ionization rate. $w(t',\beta)$ can be calculated by the molecular Ammosov-Delone-Krainov model for aligned molecules [55]:

$$\begin{aligned} w(t',\beta) = \sum_{m'} \frac{B^2(m')}{2^{|m'|}|m'|!} \\ \times \frac{1}{\kappa^{2Z_c/\kappa-1}} \left(\frac{2\kappa^3}{E(t')}\right)^{2Z_c/\kappa-|m'|-1} e^{-2\kappa^3/3E(t')}, \end{aligned} \tag{3}$$

where

$$B(m') = \sum_{l} C_l D^l_{m',m}(\beta) Q(l,m'), \tag{4}$$

$$Q(l,m) = (-1)^m \sqrt{\frac{(2l+1)(l+|m|)!}{2(l-|m|)!}}, \tag{5}$$

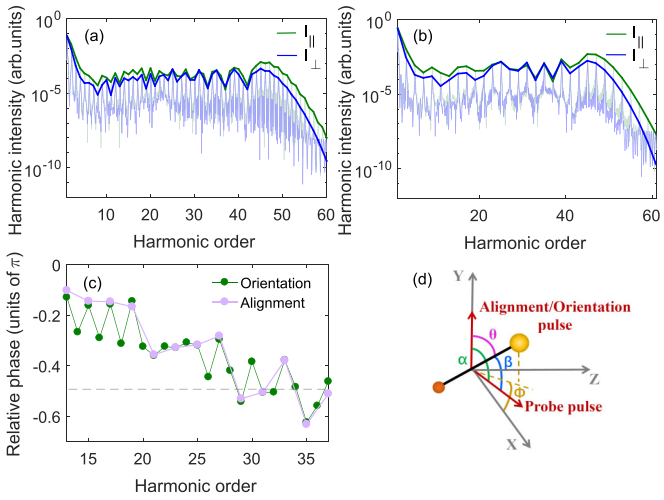

FIG. 1. (a) The parallel and perpendicular harmonic spectra for an oriented CO molecule. (b) Same as panel (a), but for an aligned CO molecule. (c) The relative phase of the parallel and perpendicular harmonic components. The green and pink lines are for the oriented and aligned CO molecules, respectively. Here, the angle β between the CO molecular axis and the polarization direction of the probe pulse is 45°. (d) A sketch of our simulation for a CO molecule.

where Z_c is the effective Coulomb charge, $\kappa = \sqrt{2I_p}$, and $D^l_{m',m}$ is the rotation matrix. The coefficients C_l for the CO molecule can be calculated by the multiple-scattering method [55,56].

$S_{\rm st}(t',t)$ is the quasiclassical action, which is given by

$$S_{\rm st}(t',t) = \int_{t'}^{t} dt'' \left\{\frac{[\mathbf{p}_{\rm st}(t',t) - \mathbf{A}(t'')]^2}{2} + I_p\right\}, \tag{6}$$

where $I_p = -0.5464$ a.u. is the ionization potential of the CO molecule. $\mathbf{p}_{\rm st}(t',t)$ is the stationary momentum, which is given by

$$\mathbf{p}_{\rm st}(t',t) = \frac{1}{t-t'} \int_{t'}^{t} \mathbf{A}(t'')dt''. \tag{7}$$

d_x and d_y are the x and y components of the dipole matrix element, which are characterized by the electron momentum $\mathbf{p} = \mathbf{p}_{\rm st} - \mathbf{A}$. Within the strong-field approximation [54], the transition dipole moment for the bound-free transition is given by

$$\mathbf{d}(\mathbf{p}) = \langle e^{-i\mathbf{p}\cdot\mathbf{r}} | \mathbf{r} | \Psi \rangle, \tag{8}$$

where Ψ is the HOMO of the CO molecule, which is obtained by an *ab initio* calculation using the GAUSSIAN09 code [57]. Then the parallel and perpendicular components of the harmonic spectrum for an oriented CO molecule are obtained by Fourier transforming the time-dependent dipole acceleration,

$$a_{\parallel}(q,\beta) = \frac{1}{T}\int_0^T \ddot{D}_{\parallel}(t,\beta) e^{-iq\omega t} dt, \tag{9}$$

$$a_{\perp}(q,\beta) = \frac{1}{T}\int_0^T \ddot{D}_{\perp}(t,\beta) e^{-iq\omega t} dt, \tag{10}$$

where T and ω are the duration and frequency of the probe pulse, respectively. q is the harmonic order. Note that for

an aligned CO molecule, the harmonic spectrum is averaged over two opposite orientation angles, i.e., $a_{\parallel,\perp}(q,\beta) = a_{\parallel,\perp}(q,\beta) + a_{\parallel,\perp}(q,\beta+\pi)$. The intensities and the phase of the parallel and perpendicular harmonic components can be given by $I_{\parallel,\perp} = |a_{\parallel,\perp}(q,\beta)|^2$ and $\phi_{\parallel,\perp} = \arg[a_{\parallel,\perp}(q,\beta)]$, respectively. Then the ellipticity of HHG is calculated by

$$\varepsilon = \sqrt{\frac{1+r^2-\sqrt{1+2r^2\cos(2\delta)+r^4}}{1+r^2+\sqrt{1+2r^2\cos(2\delta)+r^4}}}, \tag{11}$$

with the amplitude ratio $r = \frac{a_\perp(q,\beta)}{a_\parallel(q,\beta)}$ and the phase difference $\delta = \phi_\parallel - \phi_\perp$ of the parallel and perpendicular harmonic components, respectively.

It is worth mentioning that the Lewenstein model used in our simulations may be not so accurate to calculate the HHG of CO molecules and the ellipticity of HHG [58]. However, in this work, our primary objective is to gain a deeper understanding of the influence of molecular alignment and orientation on the ellipticity of HHG. In this context, the Lewenstein model remains reasonable and can isolate the impact of alignment and orientation from other effects [59,60], which are absent in the Lewenstein model.

B. Molecular alignment and orientation

In this section, we introduce the calculation model of the molecular alignment and orientation. In this model, the time-dependent molecular angular distribution $\rho(\theta,\phi,\tau)$ can be written as a weighted average of the squared modulus of the time-dependent rotational wave packet $\psi_{JM}(\theta,\phi,\tau)$, i.e.,

$$\rho(\theta,\phi,\tau) = \sum_{JM} \Gamma_{JM} |\psi_{JM}(\theta,\phi,\tau)|^2, \tag{12}$$

where θ is the angle between the molecular axis and the polarization direction of alignment or orientation pulses $\epsilon(t)$ as shown in Fig. 1(d), ϕ is the azimuthal angle in the frame of the alignment pulse, and τ is the time delay between the alignment/orientation and probe pulses. Γ_{JM} is the population of the initial state $|JM\rangle$ given by the Boltzmann distribution. Here, ρ is assumed to be constant during the probe pulse, which is reasonable since the rotation period of molecules (a few picoseconds) is usually much longer than the duration of probe pulse (tens of femtoseconds) [61]. The time-dependent rotational wave packet $\psi_{JM}(\theta,\phi,\tau)$ can be obtained by solving the time-dependent Schrödinger equation of the molecular rotational wave packet [62],

$$i\frac{\partial\psi_{JM}(\theta,\phi,\tau)}{\partial\tau} = H(t)\psi_{JM}(\theta,\phi,\tau), \tag{13}$$

with

$$H(t) = B_e J^2 - \mu\varepsilon(t)\cos\theta - \tfrac{1}{2}[(\alpha_\parallel-\alpha_\perp)\cos^2\theta + \alpha_\perp]\varepsilon^2(t) - \tfrac{1}{6}[(\beta_\parallel - 3\beta_\perp)\cos^3\theta + 3\beta_\perp\cos\theta]\varepsilon^3(t). \tag{14}$$

Here, B_e is the rotational constant, J^2 denotes the squared angular momentum operator, μ is the permanent dipole moment, $\alpha_\parallel$ and $\alpha_\perp$ are the parallel and perpendicular components of the polarizability tensor, and $\beta_\parallel$ and $\beta_\perp$ are the second-order hyperpolarizability components parallel and perpendicular to the molecular axis. For the CO molecule, $B_e = 1.93\ \mathrm{cm}^{-1}$, $\alpha_\parallel = 2.294\ \text{Å}^3$, $\alpha_\perp = 1.77\ \text{Å}^3$, $\beta_\parallel = 2.748\times10^9\ \text{Å}^5$, $\beta_\perp = 4.994\times10^8\ \text{Å}^5$, and $\mu = 0.112$ D [63,64]. Equation (13) can be solved with the split-operator method. The factor of molecular alignment and orientation is calculated by

$$\langle\cos^n\theta\rangle(\tau) = \sum_{JM}\Gamma_{JM}\langle\psi_{JM}(\theta,\phi,\tau)|\cos^n\theta|\psi_{JM}(\theta,\phi,\tau)\rangle, \tag{15}$$

where $n = 1$ is for molecular orientation and $n = 2$ is for molecular alignment.

The parallel and perpendicular components of dipole acceleration for a partially aligned/oriented CO molecular ensemble then are given by [61]

$$a'_\parallel(q,\alpha,\tau) = \int_{\phi=0}^{2\pi}\int_{\theta=0}^{\pi} a_\parallel(q,\theta)\rho(\beta,\tau)sin\theta d\theta d\phi, \tag{16}$$

$$a'_\perp(q,\alpha,\tau) = \int_{\phi=0}^{2\pi}\int_{\theta=0}^{\pi} a_\perp(q,\theta)\rho(\beta,\tau)sin\theta cos\phi d\theta d\phi, \tag{17}$$

with α of the alignment/orientation angle between the polarization directions of the alignment/orientation and probe pulses as shown in Fig. 1(d). The angle β obeys $\cos\beta = \sin\theta\sin\alpha\cos\phi + \cos\theta\cos\alpha$. It is worth noting that for the case of perfect alignment, or namely, the single-molecule response, all the molecules are aligned along the polarization direction of the alignment/orientation pulse. In this case, $\theta = 0^\circ$, and then $\alpha = \beta$. The intensity of the qth harmonic can be given by $I'_{\parallel,\perp}(q,\alpha,\tau) = |a'_{\parallel,\perp}(q,\alpha,\tau)|^2$.

III. RESULTS AND DISCUSSIONS

In Figs. 1(a) and 1(b), we present the parallel and perpendicular harmonic spectra for an oriented and an aligned CO molecule, respectively. The corresponding relative phase between the parallel and perpendicular harmonic components is shown in Fig. 1(c). Here, the angle β between the molecular axis and the polarization direction of the probe pulse is set to 45°. The probe pulse is an 800-nm linearly polarized laser field with an intensity of $3\times10^{14}\ \mathrm{W/cm^2}$. This pulse can be expressed as $E(t) = E_0 f(t)\cos(\omega t)$, where $f(t)$ is represented by a trapezoidal envelope with two-cycle rising and two-cycle falling edges, followed by an eight-cycle plateau. From Fig. 1(a), it is evident that the even harmonics are observable in the spectrum of the oriented CO molecule, owing to the asymmetry of its HOMO. Moreover, it can be observed from Figs. 1(a) and 1(b) that the intensities of the parallel and perpendicular harmonic components are comparable, while their phases are different [Fig. 1(c)]. It means that the harmonic generated from an aligned and oriented CO molecule is elliptically polarized.

We first investigate the influence of molecular alignment on EP HHG. In our simulations, we assume that a linearly polarized alignment pulse with a polarization angle α is initially applied to create molecular alignment as shown in Fig. 1(d). The alignment pulse prepares the molecule in a coherent superposition of rotational eigenstates that dephases and rephases. In the case of linear molecules, alignment recurs

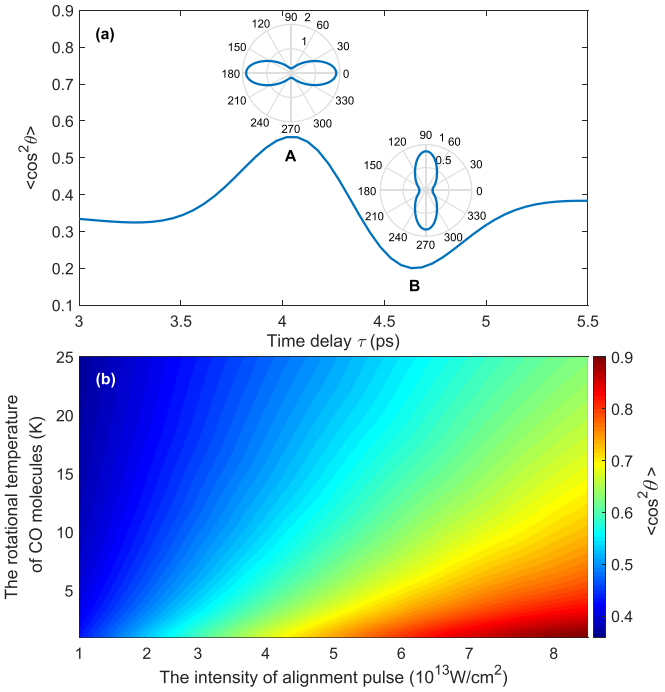

FIG. 2. (a) Evolution of the alignment factor $\langle\cos^2\theta\rangle$ with the time delay τ between the alignment and probe pulses. The intensity, wavelength, and duration of the alignment pulse are 4.5×10^{13} W/cm^2, 800 nm, and 50 fs, respectively. The molecular rotational temperature is 12.5 K. The insets are the angular distribution $\rho(\theta)$ for the aligned CO molecular ensemble at $\tau = 4.07$ and 4.63 ps. (b) The alignment factor $\langle\cos^2\theta\rangle$ at $\tau = 4.07$ ps as a function of the intensity of the alignment pulse and the rotational temperature of CO molecules.

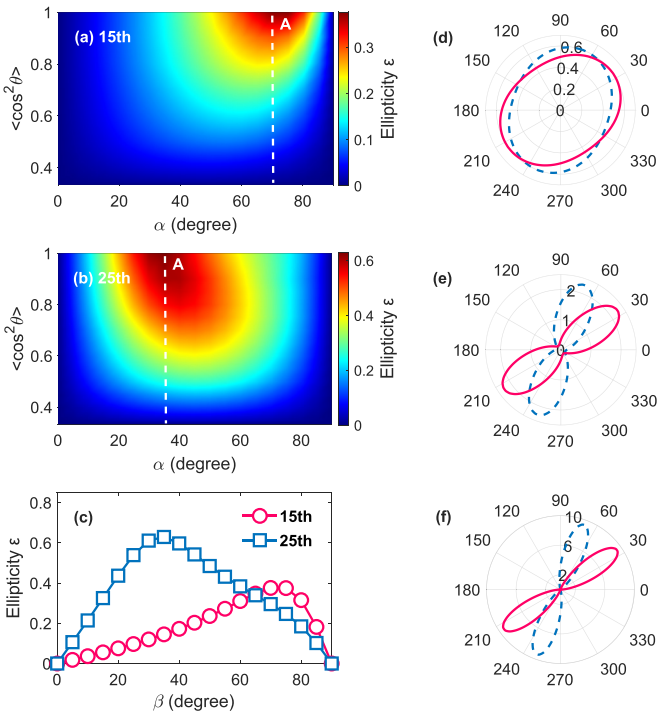

FIG. 3. (a) and (b) The ellipticity distributions of the 15th and 25th harmonics as functions of the alignment factor $\langle\cos^2\theta\rangle$ and alignment angle α for the CO molecular ensemble. (c) The ellipticities of the 15th and 25th harmonics with respect to the angle β for an individual CO molecule. (d) The angular distribution of the CO molecular ensemble for $\langle\cos^2\theta\rangle = 0.35$ and aligned at $\alpha = 70^\circ$ (blue dashed line) and 35° (red solid line). (e) and (f) Same as panel (d), but for $\langle\cos^2\theta\rangle = 0.6$ and 0.9, respectively.

periodically at multiples of the rotational period $T_{\rm rev}$. The alignment factor $\langle\cos^2\theta\rangle$ is commonly used to quantify the degree of alignment. In Fig. 2(a), we present the calculated time evolution of the alignment factor $\langle\cos^2\theta\rangle$ as a function of the time delay τ between alignment and probe pulses for the CO molecular ensemble. The intensity, the wavelength, and the duration of the alignment pulse are 4.5×10^{13} W/cm^2, 800 nm, and 50 fs, respectively. The molecular rotational temperature is 12.5 K. Notably, $\langle\cos^2\theta\rangle$ exhibits a significant dependence on the time delay τ around half rotational revival $\frac{1}{2}T_{\rm rev} = 4.32$ ps. At $\tau = 4.07$ ps, the alignment factor reaches a maximum value ($\langle\cos^2\theta\rangle = 0.55$) where the molecules are temporarily well confined within a narrow angle around the polarization direction of the alignment pulse (see inset at point A). $\langle\cos^2\theta\rangle$ reaches a minimum value at $\tau = 4.63$ ps where most molecules become perpendicular to the polarization direction of the alignment pulse (see inset at point B). Figure 2(b) shows the alignment factor $\langle\cos^2\theta\rangle$ at $\tau = 4.07$ ps as a function of the intensity of alignment pulse and the molecular rotational temperature. One can see that the alignment factor increases with the intensity of the alignment pulse and decreases with the molecular rotational temperature. However, the conditions to achieve perfect molecular alignment are very strict in experiments.

By adjusting the intensity of the alignment pulse and the molecular rotational temperature, we can obtain the different degrees of alignment as shown in Fig. 2(b). Then, we calculate the harmonic spectra for various degrees of alignment. The simulation results demonstrate that the harmonic ellipticity sensitively depends on the alignment degree and the alignment angle α. Moreover, this dependency can be split into two categories for the harmonics in the plateau region. The first type can be observed for the 11th-27th and 33rd harmonics. Here, we take the 15th and 25th harmonics as examples to show the results for the first type. Figures 3(a) and 3(b) are the ellipticity distributions of the 15th and 25th harmonics as a function of the alignment factor and the alignment angle α for the CO molecular ensemble. In this case, the harmonic ellipticity of the partially aligned CO molecular ensemble is found to be smaller than that of the individual CO molecule result [$\langle\cos^2\theta\rangle = 1$ in Figs. 3(a) and 3(b)]. Moreover, the ellipticity of HHG exhibits a monotonic increase with the degree of alignment at $\alpha = 70^\circ$ for the 15th harmonic and $\alpha = 35^\circ$ for the 25th harmonic [dashed lines in Figs. 3(a) and 3(b)]. This behavior can be understood from the alignment-angle-dependent ellipticity of the individual CO molecule [Fig. 3(c)] and the angular distribution of the CO molecular ensemble with different degrees of alignment. From Fig. 3(c), one can see that for the 15th and 25th harmonic, the harmonic ellipticity of the individual CO molecule increases with β for $\beta < 70^\circ/35^\circ$ and decreases with β for $\beta > 70^\circ/35^\circ$. Figures 3(d)–3(f) plot the angular distributions of the CO

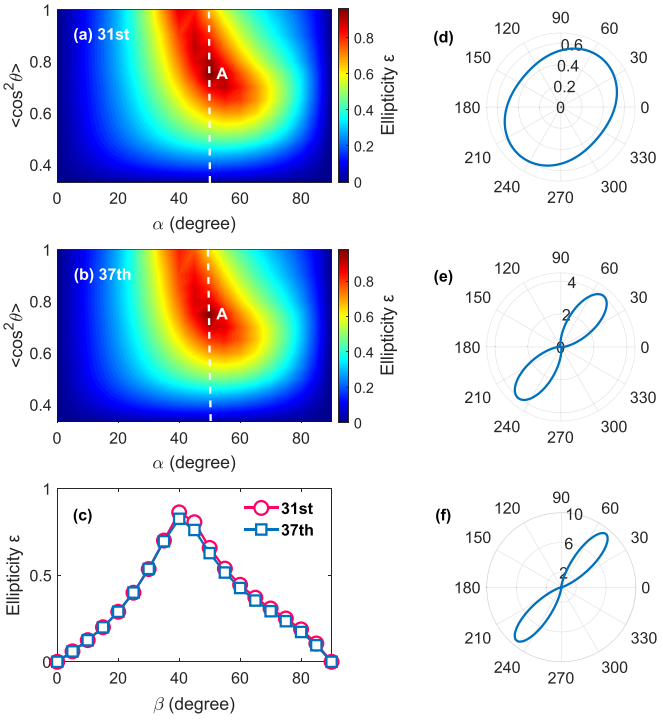

FIG. 4. (a) and (b) The ellipticity distributions of the 31st and 37th harmonics as functions of the alignment factor $\langle\cos^2\theta\rangle$ and the alignment angle α for the CO molecular ensemble. (c) The ellipticities of the 31st and 37th harmonics with respect to the angle β for an individual CO molecule. (d) The angular distribution of the CO molecular ensemble for $\langle\cos^2\theta\rangle = 0.35$ and aligned at $\alpha = 50^\circ$. (e) and (f) Same as panel (d), but for $\langle\cos^2\theta\rangle = 0.75$ and 0.9, respectively.

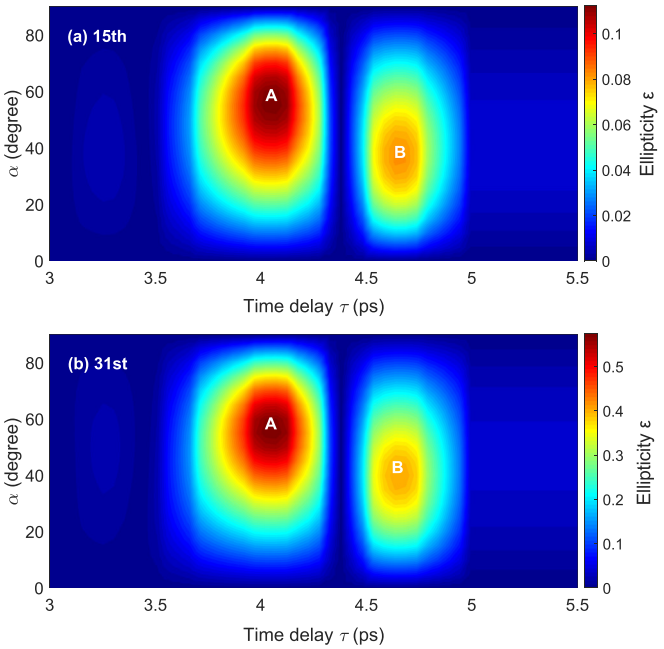

FIG. 5. (a) and (b) The ellipticity distributions of the 15th and 31st harmonics as functions of the time delay τ between the alignment and probe pulses and the alignment angle α for the CO molecular ensemble. Here, the parameters of the alignment pulse are same as those in Fig. 2(a).

molecular ensemble for different alignment factors $\langle\cos^2\theta\rangle$ of 0.35, 0.6, and 0.9 at $\alpha = 70^\circ$ (blue dashed line) and 35° (red solid line). As the alignment degree increases, the angular distribution of the CO molecular ensemble becomes narrow as shown in Figs. 3(d)–3(f). Then the contribution of CO molecules aligned around 70° for the 15th harmonic and 35° for the 25th harmonic with large ellipticity is increased. Thus, the harmonic ellipticity at 70° for the 15th harmonic and 35° for the 25th harmonic increases with the degree of alignment as shown in Figs. 3(a) and 3(b).

We next present the results for the second type, which is observed for the 29th–31st and 35th–41st harmonics. Figures 4(a) and 4(b) show the ellipticity distributions of the 31st and 37th harmonics as a function of the alignment factor $\langle\cos^2\theta\rangle$ and the alignment angle α for the CO molecular ensemble. Unlike the first type shown in Figs. 3(a) and 3(b), the harmonic ellipticity of the partially aligned CO molecular ensemble is larger than that of the individual CO molecular result [$\langle\cos^2\theta\rangle = 1$ in Figs. 4(a) and 4(b)]. Moreover, the maximum harmonic ellipticity is observed at $\alpha = 50^\circ$ and $\langle\cos^2\theta\rangle = 0.75$ [marked as point A in Figs. 4(a) and 4(b)]. When $\alpha = 50^\circ$, the ellipticity of HHG increases monotonically for $\langle\cos^2\theta\rangle < 0.75$ and turns to decrease for $\langle\cos^2\theta \gg 0.75$ [dashed lines in Figs. 4(a) and 4(b)]. Similarly, we also present the ellipticities of the 31st and 37th harmonics with respect to the angle β for the individual CO molecule in Fig. 4(c) and the angular distributions of the CO molecular ensemble aligned at 50° with different alignment factors $\langle\cos^2\theta\rangle = 0.35$, 0.75, and 0.9 in Figs. 4(d)–4(f). The ellipticity of HHG for an individual CO molecule exhibits a peak at $\beta = 40^\circ$. For a low degree of alignment, e.g., $\langle\cos^2\theta\rangle = 0.35$, the angular distribution of CO molecules is almost isotropic [Fig. 4(d)]. Consequently, the ellipticity of HHG in the CO molecular ensemble is smaller than that of the individual CO molecule result [Figs. 4(a) and 4(b)]. At the alignment factor of 0.75 [Fig. 4(e)], the molecules have a large probability to align around 40°, where the harmonic ellipticity for the individual CO molecule is maximum [Fig. 4(c)]. In this case, the ellipticity of HHG (approximately 0.96 for the 31st harmonic and 0.98 for 37th harmonic) is larger than that of the individual CO molecular result [Figs. 4(a) and 4(b)]. As the alignment factor further increases, e.g., $\langle\cos^2\theta\rangle = 0.9$, the contribution of CO molecules aligned around 40° decreases, leading to a decrease in the harmonic ellipticity in the CO molecular ensemble [Figs. 4(a) and 4(b)].

Further, we have studied the dependence of harmonic ellipticity on the time delay τ between the alignment and probe pulses in Fig. 5. The parameters for the alignment pulse and the molecular rotational temperature are the same as those used in Fig. 2(a). The ellipticity distributions as functions of τ and the alignment angle α for the CO molecular ensemble are nearly the same for all harmonics in the plateau region, such as the 15th and 31st harmonics in Figs. 5(a) and 5(b), respectively. In the region of τ from 3 to 5.5 ps, two peaks of harmonic ellipticity are observed, with one located at $\alpha = 55^\circ$ and $\tau = 4.07$ ps [marked as point A in Figs. 5(a) and 5(b)]

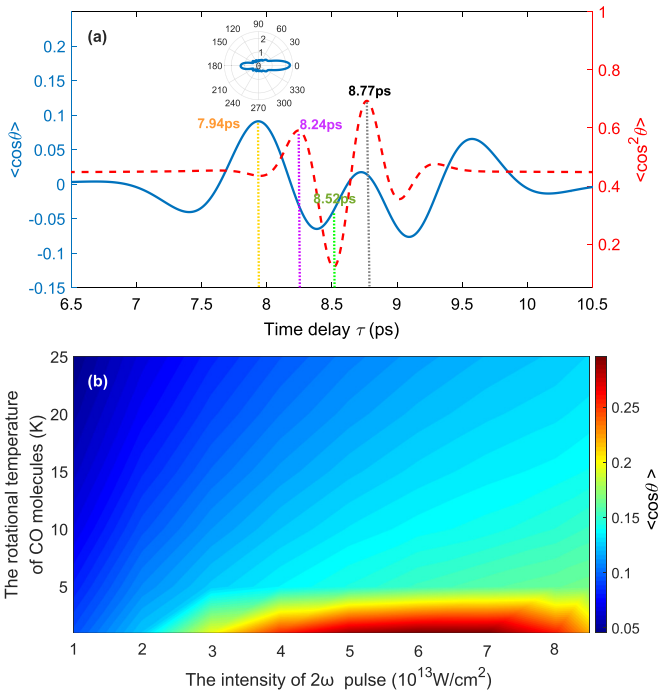

FIG. 6. (a) Evolution of the orientation factor $\langle\cos\theta\rangle$ (blue solid line) and the alignment factor $\langle\cos^2\theta\rangle$ (red dashed line) with the time delay τ between the orientation and probe pulses. The orientation pulse contains two parallel pulses. The wavelengths and intensities of these two pulses are 800 and 400 nm, 9×10^{13} and 3×10^{13} W/cm^2, respectively. The durations of these two pulses are both 70 fs. The relative phase between these two pulses is 0 and the molecular rotational temperature is 20 K. The inset is the angular distribution $\rho(\theta)$ for the oriented CO molecular ensemble at $\tau = 7.94$ ps. (b) The orientation factor $\langle\cos\theta\rangle$ at $\tau = 7.94$ ps as a function of the intensity of 2ω laser filed and the rotational temperature of CO molecules.

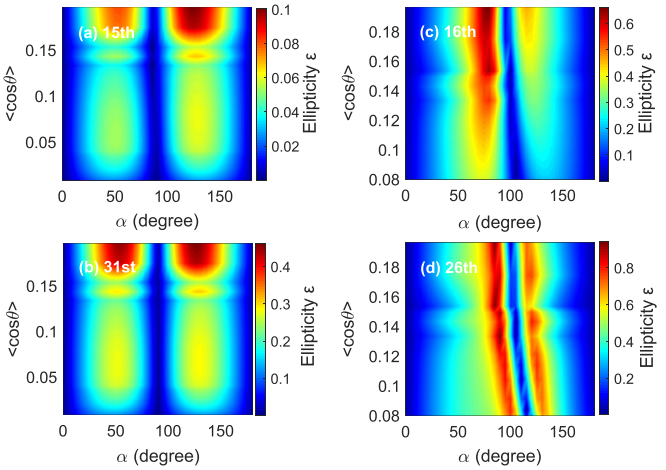

FIG. 7. (a)–(d) The ellipticity distributions of the 15th, 31st, 16th, and 26th harmonics as functions of the orientation factor $\langle\cos\theta\rangle$ and the orientation angle α for the CO molecular ensemble.

and the other at $\alpha = 35^\circ$ and $\tau = 4.63$ ps [marked as point B in Figs. 5(a) and 5(b)]. From Fig. 2, at $\tau = 4.07$ ps, $\langle\cos^2\theta\rangle$ is equal to 0.55. In this case, the maximum harmonic ellipticity is indeed located at $\alpha = 55^\circ$ as shown in Figs. 3(a) and 4(a). At $\tau = 4.63$ ps, when the alignment angle α is 35°, a large fraction of molecules are aligned at -55°. Due to the symmetry of the aligned CO molecular ensemble, the ellipticity distribution at $\alpha = -55^\circ$ is consistent with that at $\alpha = 55^\circ$. Hence, the harmonic ellipticity at $\alpha = 35^\circ$ and $\tau = 4.63$ ps is also a maximum value as shown in Fig. 5.

Next, we study the influence of the molecular orientation on EP HHG in CO molecules. Different from the molecular alignment, the molecular orientation is achieved by a linearly polarized orientation pulse composed of a carrier ω and 2ω laser fields. The orientation is reconstructed periodically at the integral multiple of the rotational period $T_{\rm rev}$. The degree of orientation is usually represented by the orientation factor $\langle\cos\theta\rangle$. In Fig. 6(a), we plot the time evolution of the orientation factor $\langle\cos\theta\rangle$ with respect to the time delay τ between orientation and probe pulses for the CO molecular ensemble (blue solid line). The wavelengths and intensities of ω and 2ω fields are 800 and 400 nm and 9×10^{13} and 3×10^{13} W/cm^2. The durations of these two pulses are both set to 70 fs and the relative phase between these two pulses is 0. Besides, the molecular rotational temperature is 20 K. As observed in Fig. 6(a), $\langle\cos\theta\rangle$ exhibits a significant dependence on the time delay τ around the full rotational revival $T_{\rm rev} = 8.64$ ps. It reaches a maximum at $\tau = 7.94$ ps where most molecules are oriented well along the polarization direction of the orientation pulse. By changing the intensity of the 2ω pulse and the molecular rotational temperature, we can obtain different orientation factors $\langle\cos\theta\rangle$ at $\tau = 7.94$ ps as shown in Fig. 6(b).

We next calculated the ellipticity distributions of the CO molecular ensemble at different degrees of orientation. Figures 7(a)–7(d) present the results for the 15th, 31st, 16th, and 26th harmonics. It is worth noting that the appearance of even harmonics is mainly determined by the asymmetry of the CO molecular ensemble. When $\langle\cos\theta\rangle < 0.08$, the asymmetry of the CO molecular ensemble is not obvious and then the even harmonics is very weak. Therefore, for the 16th [Fig. 7(c)] and the 26th [Fig. 7(d)] harmonics, we only present the ellipticity distributions for $\langle\cos\theta \gg 0.08$. One can see that the harmonic ellipticity sensitively depends on the degree of orientation, and a large harmonic ellipticity of 0.8 can be achieved at a moderate orientation factor of $\langle\cos\theta\rangle = 0.1$ for the 26th harmonic.

In Fig. 8, we study the dependence of harmonic ellipticity on the time delay τ between orientation and probe pulses. The parameters of the orientation pulse and the molecular rotational temperature are the same as those in Fig. 6(a). From Fig. 6(a), one can see that the even harmonic is generated only in a small time interval (7.86 ps $< \tau <$ 8.01 ps). Therefore, we only present the results for odd harmonics in the plateau region, such as the 15th [Fig. 8(a)] and the 31st [Fig. 8(b)] harmonics. One can see that the harmonic ellipticity is much larger around the full rotational revival $T_{\rm rev} = 8.64$ ps, such as at 8.24, 8.52, and 8.77 ps. At these three moments, the CO molecules exhibit poor orientation [see blue solid line in Fig. 6(a)] but good alignment [see red dashed line in Fig. 6(a)]. While at 7.94 ps, the ellipticity is smaller than that at the aforementioned moments, where the orientation factor of the CO molecular ensemble reaches its maximum, but the alignment degree of the CO molecular ensemble is low

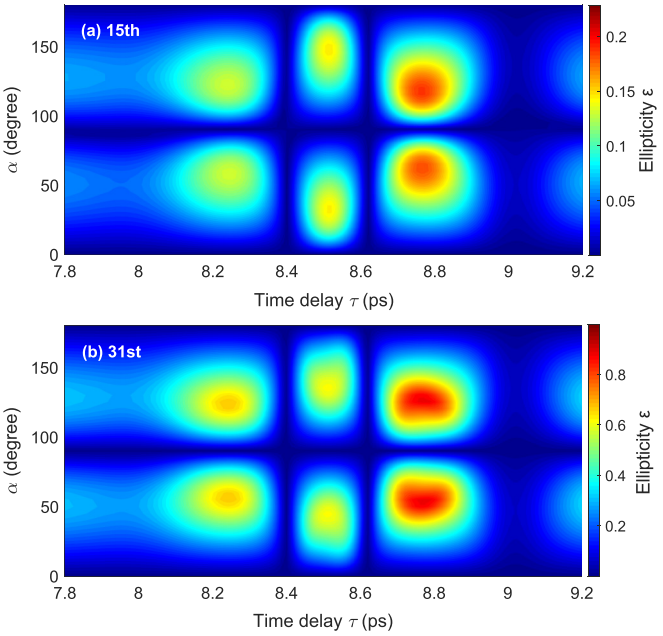

FIG. 8. (a) and (b) The ellipticity distributions of the 15th and 31st harmonics as functions of the time delay τ between orientation and probe pulses and the orientation angle α for the CO molecular ensemble. Here, the parameters of the orientation pulse are same as those in Fig. 6(a).

[see Fig. 6(a)]. The degree of molecular alignment reflects the concentration of the molecular ensemble, while the degree of molecular orientation reflects the asymmetry of the molecular ensemble. Thus, it can be seen that the harmonic ellipticity is mainly influenced by the concentration degree rather than the asymmetry degree.

IV. CONCLUSION

In conclusion, we study the impact of molecular alignment and orientation on the EP HHG of CO molecules. The results show that the molecular alignment and orientation play a significant role in EP HHG. For the aligned CO molecular ensemble, a large HHG ellipticity of $\varepsilon = 0.98$ can be obtained at an alignment factor of $\langle\cos^2\theta\rangle = 0.75$. For the oriented CO molecular ensemble, a large harmonic ellipticity of 0.8 can be achieved at a moderate orientation factor of $\langle\cos\theta\rangle = 0.1$. Note that due to the limitation of the Lewenstein's model, there may be a discrepancy between the theoretical calculated ellipticity of harmonics in an aligned ensemble of molecules here between the experiment studies. Our results give a deeper understanding of the influence of molecular alignment and orientation on the ellipticity of HHG.

ACKNOWLEDGMENTS

This work was supported by Guangdong Major Project of Basic and Applied Basic Research (Grant No. 2019B030302003); the National Natural Science Foundation of China under Grants No. 12104349, No. 12204279, and No. 12174295; and the Campus Science Foundation Research Project of Wuhan Institute of Technology, China (Grant No. K2021076).

[1] A. McPherson, G. Gibson, H. Jara, U. Johann, T. S. Luk, I. A. McIntyre, K. Boyer, and C. K. Rhodes, J. Opt. Soc. Am. B **4**, 595 (1987).
[2] E. Goulielmakis, M. Schultze, M. Hofstetter, V. S. Yakovlev, J. Gagnon, M. Uiberacker, A. L. Aquila, E. M. Gullikson, D. T. Attwood, R. Kienberger, F. Krausz, and U. Kleineberg, Science **320**, 1614 (2008).
[3] J. Li, X. Ren, Y. Yin, K. Zhao, A. Chew, Y. Cheng, E. Cunningham, Y. Wang, S. Hu, Y. Wu, M. Chini, and Z. Chang, Nat. Commun. **8**, 186 (2017).
[4] X. Wang, L. Wang, F. Xiao, D. Zhang, Z. Lü, J. Yuan, and Z. Zhao, Chin. Phys. Lett. **37**, 023201 (2020).
[5] M. Hentschel, R. Kienberger, Ch. Spielmann, G. A. Reider, N. Milosevic, T. Brabec, P. Corkum, U. Heinzmann, M. Drescher, and F. Krausz, Nature (London) **414**, 509 (2001).
[6] H. Ahmadi, E. Plésiat, M. Moioli, F. Frassetto, L. Poletto, P. Decleva, C. D. Schröter, T. Pfeifer, R. Moshammer, A. Palacios, F. Martin, and G. Sansone, Nat. Commun. **13**, 1242 (2022).
[7] J. Itatani, J. Levesque, D. Zeidler, H. Niikura, H. Pépin, J. C. Kieffer, P. B. Corkum, and D. M. Villeneuve, Nature (London) **432**, 867 (2004).
[8] M. I. Stockman, M. F. Kling, U. Kleineberg, and F. Krausz, Nat. Photon. **1**, 539 (2007).
[9] L. He, X. Zhu, W. Cao, P. Lan, and P. Lu, Chin. Phys. B **31**, 123301 (2022).
[10] F. Frassetto, C. Cacho, C. A. Froud, I. C. E. Turcu, P. Villoresi, W. A. Bryan, E. Springate, and L. Poletto, Opt. Express **19**, 19169 (2011).
[11] Y. Mairesse, A. de Bohan, L. J. Frasinski, H. Merdji, L. C. Dinu, P. Monchicourt, P. Breger, M. Kovacev, R. Taïeb, B. Carré, H. G. Muller, P. Agostini, and P. Salières, Science **302**, 1540 (2003).
[12] A. Ferré, C. Handschin, M. Dumergue, F. Burgy, A. Comby, D. Descamps, B. Fabre, G. A. Garcia, R. Géneaux, L. Merceron, E. Mével, L. Nahon, S. Petit, B. Pons, D. Staedter, S. Weber, T. Ruchon, V. Blanchet, and Y. Mairesse, Nat. Photon. **9**, 93 (2014).
[13] T. Fan, P. Grychtol, R. Knut, C. Hernández-Garca, D. D. Hickstein, D. Zusin, C. Gentry, F. J. Dollar, C. A. Mancuso, C. W. Hogle *et al.*, Proc. Natl. Acad. Sci. USA **112**, 14206 (2015).
[14] M. Negro, M. Devetta, D. Faccial, S. De. Silvestri, C. Vozzi, and S. Stagira, Faraday Discuss. **171**, 133 (2014).
[15] M. V. Frolov, N. L. Manakov, T. S. Sarantseva, and A. F. Starace, Phys. Rev. A **86**, 063406 (2012).
[16] T. S. Sarantseva, A. A. Silaev, and N. L. Manakov, J. Phys. B **50**, 074002 (2017).
[17] F. J. Sun, C. Chen, W. Y. Li, X. Liu, W. Li, and Y. J. Chen, Phys. Rev. A **103**, 053108 (2021).
[18] D. Habibović and D. B. Milošević, Photonics **7**, 110 (2020).

[19] X. X. Huo, Y. H. Xing, T. Qi, Y. Sun, B. Li, J. Zhang, and X. S. Liu, Phys. Rev. A **103**, 053116 (2021).

[20] B. Mahieu, S. Stremoukhov, D. Gauthier, C. Spezzani, C. Alves, B. Vodungbo, P. Zeitoun, V. Malka, G. De Ninno, and G. Lambert, Phys. Rev. A **97**, 043857 (2018).

[21] Y. Fang and Y. Liu, Phys. Rev. A **103**, 033116 (2021).

[22] K. M. Dorney, J. L. Ellis, C. Hernández-García, D. D. Hickstein, C. A. Mancuso, N. Brooks, T. Fan, G. Fan, D. Zusin, C. Gentry, P. Grychtol, H. C. Kapteyn, and M. M. Murnane, Phys. Rev. Lett. **119**, 063201 (2017).

[23] N. Zhavoronkov and M. Ivanov, Opt. Lett. **42**, 4720 (2017).

[24] C. Hernández-García, C. G. Durfee, D. D. Hickstein, T. Popmintchev, A. Meier, M. M. Murnane, H. C. Kapteyn, I. J. Sola, A. Jaron-Becker, and A. Becker, Phys. Rev. A **93**, 043855 (2016).

[25] J. L. Ellis, K. M. Dorney, D. D. Hickstein, N. J. Brooks, C. Gentry, C. Hernández-García, D. Zusin, J. M. Shaw, Q. L. Nguyen, C. A. Mancuso, G. S. M. Jansen, S. Witte, H. C. Kapteyn, and M. M. Murnane, Optica **5**, 479 (2018).

[26] P. C. Huang, C. Hernández-García, J. T. Huang, P. Y. Huang, C. H. Lu, L. Rego, D. D. Hickstein, J. L. Ellis, A. Jaron-Becker, A. Becker, S. D. Yang, C. G. Durfee, L. Plaja, H. C. Kapteyn, M. M. Murnane, A. H. Kung, and M. C. Chen, Nat. Photon. **12**, 349 (2018).

[27] A. R. Madhani, E. Irani, and M. Monfared, Opt. Express **31**, 18430 (2023).

[28] S. Eckart, M. Kunitski, M. Richter, A. Hartung, J. Rist, F. Trinter, K. Fehre, N. Schlott, K. Henrichs, L. P. H. Schmidt, T. Jahnke, M. Schöfflfler, K. Liu, I. Barth, J. Kaushal, F. Morales, M. Ivanov, O. Smirnova, and R. Dörner, Nat. Phys. **14**, 701 (2018).

[29] D. Wang, X. Zhu, H. Yuan, P. Lan, and P. Lu, Phys. Rev. A **101**, 023406 (2020).

[30] C. Zhai, X. Zhu, J. Long, R. Shao, Y. Zhang, L. He, Q. Tang, Y. Li, P. Lan, B. Yu, and P. Lu, Phys. Rev. A **103**, 033114 (2021).

[31] X. Zhou, R. Lock, N. Wagner, W. Li, H. C. Kapteyn, and M. M. Murnane, Phys. Rev. Lett. **102**, 073902 (2009).

[32] S. K. Son, D. A. Telnov, and S.-l. Chu, Phys. Rev. A **82**, 043829 (2010).

[33] H. Du, L. Luo, X. Wang, and B. Hu, Phys. Rev. A **86**, 013846 (2012).

[34] O. Smirnova, S. Patchkovskii, Y. Mairesse, N. Dudovich, D. Villeneuve, P. Corkum, and M. Y. Ivanov, Phys. Rev. Lett. **102**, 063601 (2009).

[35] Y. Xia and A. Jaroń-Becker, Opt. Lett. **39**, 1461 (2014).

[36] H. Sakai, C. P. Safvan, J. J. Larsen, K. M. Hilligsoe, K. Hald, and H. Stapelfeldt, J. Chem. Phys **110**, 10235 (1999).

[37] W. Tao, S. Sun, L. He, Y. He, J. Hu, Y. Deng, C. Xu, P. Lan, and P. Lu, Chin. Opt. Lett. **21**, 120021 (2023).

[38] Y. He, L. He, P. Wang, B. Wang, S. Sun, R. Liu, B. Wang, P. Lan, and P. Lu, Opt. Express **28**, 21182 (2020).

[39] Y. He, L. He, P. Lan, B. Wang, L. Li, X. Zhu, W. Cao, and P. Lu, Phys. Rev. A **99**, 053419 (2019).

[40] R. Velotta, N. Hay, M. B. Mason, M. Castillejo, and J. P. Marangos, Phys. Rev. Lett. **87**, 183901 (2001).

[41] S. De, I. Znakovskaya, D. Ray, F. Anis, N. G. Johnson, I. A. Bocharova, M. Magrakvelidze, B. D. Esry, C. L. Cocke, I. V. Litvinyuk, and M. F. Kling, Phys. Rev. Lett. **103**, 153002 (2009).

[42] K. Oda, M. Hita, S. Minemoto, and H. Sakai, Phys. Rev. Lett. **104**, 213901 (2010).

[43] S. Fleischer, Y. Zhou, R. W. Field, and K. A. Nelson, Phys. Rev. Lett. **107**, 163603 (2011).

[44] K. Kitano, N. Ishii, N. Kanda, Y. Matsumoto, T. Kanai, M. Kuwata-Gonokami, and J. Itatani, Phys. Rev. A **88**, 061405(R) (2013).

[45] M. Lapert and D. Sugny, Phys. Rev. A **85**, 063418 (2012).

[46] C. C. Shu and N. E. Henriksen, Phys. Rev. A **87**, 013408 (2013).

[47] B. Friedrich and D. Herschbach, J. Chem. Phys. **111**, 6157 (1999).

[48] U. Buck and M. Farnik, Int. Rev. Phys. Chem. **25**, 583 (2006).

[49] A. Goban, S. Minemoto, and H. Sakai, Phys. Rev. Lett. **101**, 013001 (2008).

[50] S. Sun, Y. He, L. He, J. Hu, P. Lan, and P. Lu, Phys. Rev. A **107**, 033105 (2023); S. Sun, L. He, C. Xu, Y. Deng, P. Lan, and P. Lu, *ibid.* **109**, 033105 (2024).

[51] L. He, S. Sun, P. Lan, Y. He, B. Wang, P. Wang, X. Zhu, L. Li, W. Cao, P. Lu, and C. D. Lin, Nat. Commun. **13**, 4595 (2022).

[52] L. He, Y. He, S. Sun, E. Goetz, A.-T. Le, X. Zhu, P. Lan, P. Lu, and C. D. Lin, Adv. Photon. **5**, 056001 (2023).

[53] A.-T. Le, R. R. Lucchese, and C. D. Lin, Phys. Rev. A **82**, 023814 (2010).

[54] M. Lewenstein, Ph. Balcou, M. Yu. Ivanov, A. L'Huillier, and P. B. Corkum, Phys. Rev. A **49**, 2117 (1994).

[55] X. M. Tong, Z. X. Zhao, and C. D. Lin, Phys. Rev. A **66**, 033402 (2002).

[56] D. Dill and J. L. Dehmer, J. Chem. Phys. **61**, 692 (1974).

[57] M. J. Frisch, G. W. Trucks, H. B. Schlegel *et al.*, *Computer Code* GAUSSIAN09, *Rev. D.01*. (Gaussian, Inc., Wallingford, CT, 2009).

[58] A. Etches, C. B. Madsen, and L. B. Madsen, Phys. Rev. A **81**, 013409 (2010).

[59] C.-T. Le, V.-H. Hoang, L.-P. Tran, and V.-H. Le, Phys. Rev. A **97**, 043405 (2018).

[60] S. Ohmura, T. Kato, T. Oyamada, S. Koseki, H. Ohmura, and H. Kono, J. Phys. B **51**, 034001 (2018).

[61] A.-T. Le, R. R. Lucchese, S. Tonzani, T. Morishita, and C. D. Lin, Phys. Rev. A **80**, 013401 (2009).

[62] T. Kanai and H. Sakai, J. Chem. Phys. **115**, 5492 (2001).

[63] K. A. Peterson and T. H. Dunning, Jr., J. Mol. Struct.: THEOCHEM **400**, 93 (1997).

[64] M. Pecul, Chem. Phys. Lett. **404**, 217 (2005).